Volume 6
Number 11
November 2025
Pages 1659–1824

RSC Chemical Biology

rsc.li/rsc-chembio

ISSN 2633-0679

ROYAL SOCIETY OF CHEMISTRY

COMMUNICATION

Hidetomo Yokoo, Yosuke Demizu *et al.*
Reductively activated CPP–PROTAC nanocomplexes enhance target degradation *via* efficient cellular uptake

RSC Chemical Biology

ROYAL SOCIETY OF CHEMISTRY

COMMUNICATION

View Article Online
View Journal | View Issue

Cite this: *RSC Chem. Biol.*, 2025, **6**, 1705

Received 30th July 2025,
Accepted 22nd August 2025

DOI: 10.1039/d5cb00196j

rsc.li/rsc-chembio

Reductively activated CPP–PROTAC nanocomplexes enhance target degradation *via* efficient cellular uptake

Maho Miyamoto,[ab] Kosuke Saito,[c] Hidetomo Yokoo*[b] and Yosuke Demizu *[abd]

We developed a nanoparticle based on a cell-penetrating peptide-PROTAC conjugate with a disulfide linker, *MZ1-R9*, and dextran sulfate, enhancing cellular uptake and BRD4 degradation. This delivery platform significantly improves PROTAC bioavailability and offers a promising strategy to overcome membrane permeability challenges for targeted protein degradation.

The proteolysis-targeting chimeras (PROTACs) are a novel therapeutic that enables the selective degradation of disease-related proteins *via* the ubiquitin–proteasome system.[1–4] PROTACs induce proteasomal degradation of target proteins particularly in oncology. PROTAC comprises two ligands—one that binds to an E3 ubiquitin ligase and another that recognizes a protein of interest (POI)—connected by a linker. Despite their therapeutic potential, with over 40 PROTACs currently being evaluated in clinical trials, including the estrogen receptor–targeting ARV-471 (Phase 3; ClinicalTrials.gov Identifier: NCT05909397),[5] the clinical translation of PROTACs remains hindered by intrinsic physicochemical limitations.

PROTACs commonly exhibit large molecular weights (typically > Mw 800) and low membrane permeability.[6] Notably, even minimized PROTACs often exceed Mw 650,[7] leading to suboptimal pharmacokinetics. For instance, ***MZ1***—a well-characterized BRD4-targeting PROTAC[8] shows PAMPA permeability approximately 190-fold lower than its POI ligand JQ1 and 290-fold lower than the E3 ligand VH032.[9] To address these challenges, several chemical modification strategies have been explored to improve the drug-like properties of PROTACs.[10] Although extensive structure–activity relationship (SAR) studies of each PROTAC candidate, such as replacing amides with esters, or introducing conformational constraints, are useful,[11] cell-penetrating peptides (CPPs) offer another versatile delivering platform for otherwise impermeable cargos, including proteins, nucleic acids, and nanoparticles into cells.[12] CPPs are short, typically cationic peptides (<30 amino acids) capable of translocating across the cell membrane, even at low concentrations.[13] Inspired by these capabilities, CPPs have been extensively investigated for their potential in enhancing drug delivery platforms, including peptide–drug conjugates (PDCs) and antibody–drug conjugates (ADCs), aiming to improve pharmacokinetics, target selectivity, and intracellular accessibility.[14] This approach is consistent with the broader strategy of targeted delivery systems designed to increase the pharmacological precision of therapeutic agents.[15] For example, CPP-conjugated peptide-based PROTACs have been reported by conjugating a targeting peptide for cancer.[16–18]

Nanoparticles are superior in controlling blood circulation, and therefore, high functionality has been developed using peptide-based nanoparticles as well as in the case of PROTAC.[19,20] Nanoparticle-based delivery systems are also expected to increase the versatility of CPP-PROTACs without altering their molecular structures. These systems possibly improve cell permeability and toxicity of CPP by decreasing the required compound dosage and enable targeted delivery through functionalization similar to recent studies which have successfully applied various nanocarriers, including liposomes, polymeric micelles, and inorganic particles, for delivering PROTACs.[21,22]

In this study, we aimed to develop a delivery system that integrates CPP conjugation and nanoparticle formation to improve intracellular delivery and therapeutic efficacy of PROTACs. We designed ***MZ1-R9***, a conjugate of the model PROTAC, ***MZ1*** and the cationic nonaarginine (***R9***)[23] CPP, linked *via* a disulfide bond that is cleavable under reductive intracellular conditions. This conjugate was subsequently complexed with dextran sulfate (***DS***)—a biocompatible anionic polysaccharide—*via* electrostatic interactions to form nanoparticles.[24] The resulting nanocomplex enhances cellular uptake and

[a] *Graduate School of Medical Life Science, Yokohama City University, 1-7-29 Yokohama 230-0045, Japan*
[b] *Division of Organic Chemistry, National Institute of Health Sciences, 3-25-26 Tonomachi, Kawasaki 210-9501, Japan. E-mail: yokoo@nihs.go.jp, demizu@nihs.go.jp*
[c] *Division of Medicinal Safety Science, National Institute of Health Sciences, 3-25-26, Tonomachi, Kawasaki 210-9501, Japan*
[d] *Graduate School of Medicine, Dentistry and Pharmaceutical Sciences, Okayama University, Okayama, Japan*

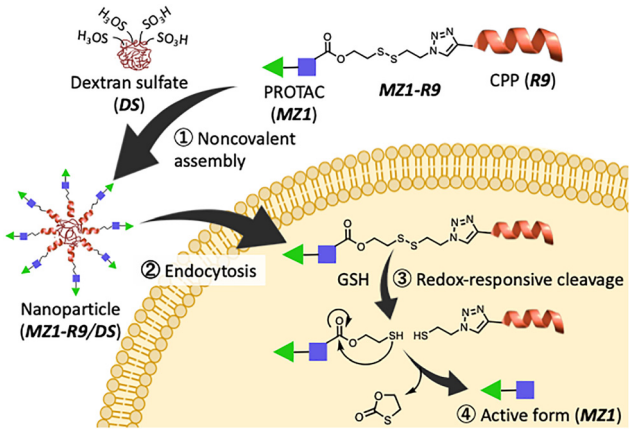

Fig. 1 Schematic representation of the intracellular release mechanism of ***MZ1-R9/DS*** nanoparticles. Upon cellular entry, glutathione (GSH) reduces the disulfide bond, activating ***MZ1-R9*** and releasing the active PROTAC, ***MZ1***.

intracellular release of the active PROTAC moiety, potentially overcoming key delivery challenges and enabling broader therapeutic applications of PROTAC technology. This nanocomplex enhances cellular uptake *via* endocytosis and releases the active PROTAC intracellularly upon disulfide bond cleavage by glutathione (GSH) (Fig. 1). This strategy addresses key delivery challenges of PROTACs by enhancing membrane permeability through nanoparticle formulation of the peptide-PROTAC conjugate.

MZ1-R9 was synthesized *via* copper(I)-catalyzed azide–alkyne cycloaddition (CuAAC) between ***MZ1*** bearing a terminal azide on a disulfide linker and ***R9*** modified at its N-terminus with an alkyne group. To evaluate cellular uptake behavior, a fluorescent analog, ***FAM-R9***, was synthesized by substituting the ***MZ1*** moiety with 5(6)-carboxyfluorescein, as shown in Scheme 1.

The size and zeta potential of the complexes were measured by DLS in 10 mM HEPES buffer (pH 7.3) to assess their physicochemical properties (Table S1). The charge ratio (N/S ratio) is defined as the molar ratio of protonatable nitrogen (N) groups in the peptide to sulfo (S) groups in ***DS***. The fluorescence intensity of ***FAM-R9/DS*** complexes increased at N/S from 1, indicating formation of complexes was saturated at N/S of 1 (Fig. S6). ***FAM-R9/DS*** complexes were prepared at N/S ratios of 1, 2, 4, and 8, and their hydrodynamic size and surface charge were characterized by different techniques (DLS for N/S = 1 to 8 and NTA for N/S = 1, Table S1 and Fig. S7). All complexes exhibited hydrodynamic diameters below 200 nm, with PDI values consistently less than 0.4, indicating moderate size distributions typically considered acceptable for nanoparticle formulations. The particle size and PDI remained relatively constant across the tested N/S ratios, indicating stable nanoparticle formation over the examined range. In contrast, the zeta potential increased with increasing charge ratio, rising from +22.6 mV at N/S = 1 to +36.7 mV at N/S = 8. Furthermore, ***MZ1-R9/DS*** complexes exhibited small particle sizes below 100 nm, suggesting the formation of stable and compact nanoparticles that are favorable to efficient cellular internalization.

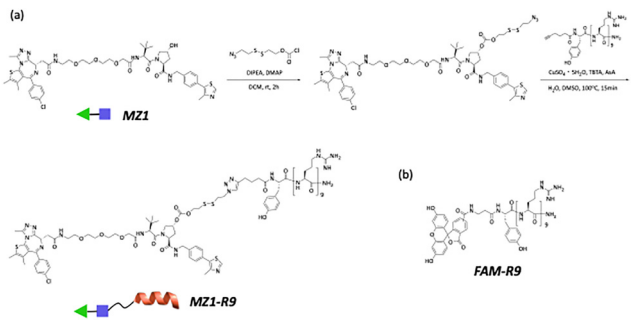

Scheme 1 Synthesis of (a) ***MZ1-R9*** and (b) chemical structure of ***FAM-R9***.

Intracellular fluorescence of ***FAM-R9/DS*** complexes was measured to assess cellular uptake in MCF-7 cells. Fluorescence intensity in MCF-7 cells was quantified by flow cytometry after 24 hours of treatment (Fig. 2 and Fig. S8). The ***FAM-R9/DS*** complex (N/S = 1) exhibited significantly enhanced cellular uptake, with fluorescence intensity approximately five times higher than that of free ***FAM-R9*** ($p < 0.001$). These results suggest that nanoparticle formation enhances peptide stability and markedly promotes its intracellular uptake. Furthermore, the uptake of ***DS*** as a function of the N/S ratio was evaluated using fluorescently labeled ***DS*** (Fig. S9). To ensure that the physicochemical properties of the complex matched those of ***FAM-R9/DS***, ***R9*** was labeled with 5-nitrofluorescein (***5-NO$_2$-FAM***)—a structural analog of FAM that lacks fluorescence—yielding ***5-NO$_2$-FAM-R9***. The highest cellular uptake was observed at an N/S = 1, mirroring the uptake profile of the peptide. These findings indicate that ***DS***, along with the peptide, is internalized as nanoparticulate complexes. Taken together, these results highlight the importance of N/S ratio optimization in the design of nanocarriers for efficient intracellular delivery. Based on these findings, subsequent experiments were conducted using N/S ratios of 1 and 8.

Time-dependent intracellular uptake of ***FAM-R9*** and ***FAM-R9/DS*** complexes was evaluated using flow cytometry (Fig. S10). The ***FAM-R9/DS*** complex (N/S = 1) exhibited markedly higher

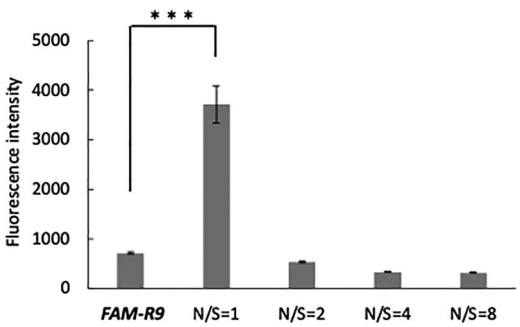

Fig. 2 Intracellular uptake of ***FAM-R9*** and ***FAM-R9/DS*** complexes in MCF-7 cells. The peptide concentration was fixed at 2 μM across all conditions, with varying volumes of 8 μM ***DS*** solution corresponding to N/S ratios of 1 (30 μL), 2 (15 μL), 4 (7.5 μL), and 8 (3.8 μL). Fluorescence intensity was measured by flow cytometry following incubation with free ***FAM-R9*** or ***FAM-R9/DS*** complexes at different N/S ratios ($n = 3$, mean ± SD, ***$p < 0.001$).

intracellular uptake than both free ***FAM-R9*** and the complex at N/S = 8, with maximal accumulation observed at 12 hours post-treatment. This complex consistently maintained the highest intracellular uptake even after 24 hours, indicating superior and sustained cellular internalization at N/S = 1.

To elucidate the uptake mechanism, MCF-7 cells were treated with three endocytosis inhibitors: amiloride (5 mM), methyl-β-cyclodextrin (MβCD, 10 mM), and sucrose (0.4 M). Each inhibitor selectively blocks a distinct endocytic pathway: amiloride for macropinocytosis, MβCD for caveolae-mediated endocytosis, and sucrose for clathrin-mediated endocytosis.[25,26] MCF-7 cells were pretreated with each inhibitor at 37 °C for 30 minutes, followed by incubation with ***FAM-R9*** or the ***FAM-R9/DS*** complex (N/S = 1) for an additional 30 minutes. Intracellular fluorescence was then quantified. The uptake of both ***FAM-R9*** and its ***DS*** complex was significantly reduced by all three inhibitors, indicating that their cellular entry occurs predominantly *via* endocytosis (Fig. 3). Intracellular localization was examined by fluorescence microscopy. After 2 hours of treatment with the ***FAM-R9/DS*** complex (N/S = 1), minimal overlap between ***FAM-R9/DS*** signals and LysoTracker Red was observed, suggesting that punctate fluorescence pattern implies that the complex may remain in particulate form, which could potentially hinder the efficient cytosolic release of ***MZ1*** (Fig. S11). Nonetheless, a fraction of the complex may be released from endosomes or lysosomes.

The *in vitro* stability of ***MZ1-R9*** under physiologically relevant conditions was evaluated. ***MZ1-R9*** and the ***MZ1-R9/DS*** complex (N/S = 1) were dissolved in PBS containing 5 mM GSH at a final concentration of 100 nM and incubated at 37 °C. Aliquots were collected at different time points for UHPLC analysis. As shown in the drug release profiles (Table 1), free ***MZ1-R9*** exhibited a rapid burst release of ***MZ1*** within the first 30 minutes under reductive conditions, with nearly complete conversion to free ***MZ1***. In contrast, the ***MZ1-R9/DS*** complex (N/S = 1) showed a sustained release profile, retaining approximately 13% of the intact conjugate after 6 hours. In addition, ***MZ1-R9/DS*** was more stable in serum-containing medium than

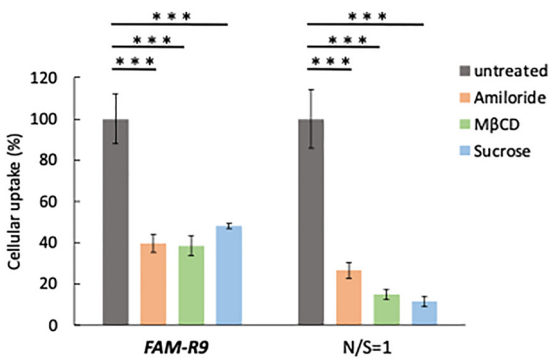

Fig. 3 Mechanistic analysis of cellular uptake of ***FAM-R9*** and the ***FAM-R9/DS*** complex (N/S = 1) in MCF-7 cells using endocytosis inhibitors: amiloride (5 mM, macropinocytosis inhibitor), methyl-β-cyclodextrin (MβCD, 10 mM, caveolae-mediated endocytosis inhibitor), and sucrose (0.4 M, clathrin-mediated endocytosis inhibitor). Data are expressed as mean ± SD (n = 3), ***$p < 0.001$.

Table 1 UHPLC analysis of ***MZ1-R9*** and the ***MZ1-R9/DS*** complex (N/S = 1) after incubation in PBS containing 5 mM GSH at 37 °C. The peak areas of ***MZ1-R9*** and released ***MZ1*** were normalized to 100%

	Time (h)	***MZ1-R9*** (%)	***MZ1*** (%)
MZ1-R9	0	100	0
	0.5	0	100
	1	0	100
	2	0	100
	6	0	100
	24	0	100
MZ1-R9/DS (N/S = 1)	0	100	0
	0.5	32.9	67.1
	1	16.9	83.1
	2	30.6	69.4
	6	12.7	87.3
	24	0	100

MZ1-R9 (Fig. S13 and Table S2). These results indicate that the nanocomplex exhibits enhanced *in vitro* stability and enables gradual PROTAC release, supporting its potential for sustained intracellular delivery.

We next evaluated the BRD4 degradation activity of ***MZ1-R9*** and its ***DS*** complexes using western blot analysis in MCF-7 cells. Cells were treated with the compounds, and BRD4 expression levels were subsequently assessed. To allow sufficient time for intracellular uptake, endosomal escape, disulfide bond reduction, and subsequent release and target degradation, the experimental protocol was modified accordingly. Cells were treated with the compounds, followed by PBS washing to remove extracellular components. Following PBS washes at each time point, cells were further incubated for 24 hours to allow sufficient time for complete BRD4 degradation (Fig. 4a).

Time-course analysis revealed that neither ***MZ1-R9*** nor the ***MZ1-R9/DS*** complex (N/S = 1) induced detectable BRD4 degradation after 6 hours of treatment. However, after 12 hours, the N/S = 1 complex exhibited BRD4 degradation comparable to that of unconjugated ***MZ1***. Furthermore, at both 12 and 24 hours, the N/S = 1 complex induced greater BRD4 degradation than ***MZ1-R9*** alone, suggesting that nanoparticle formation facilitated improved intracellular delivery and enhanced degradation efficiency (Fig. 4b–d).

To further assess intracellular delivery efficiency, we performed LC-MS/MS analysis. MCF-7 cells were treated with 100 nM of either free ***MZ1*** or the ***MZ1-R9/DS*** complex (N/S = 1) for 12 hours, followed by 24-hour incubation to ensure complete uptake and intracellular processing. LC-MS/MS quantification revealed that nanoparticle formation enhanced intracellular ***MZ1*** levels by approximately 4-fold compared to free ***MZ1***. Specifically, free ***MZ1*** achieved a cellular uptake of 0.049% of the administered dose, whereas the ***MZ1-R9/DS*** complex (N/S = 1) reached 0.21%, confirming improved cellular accumulation (Fig. 5).

Our CPP-conjugated PROTAC nanoparticles enhance intracellular delivery and target protein degradation through a dual mechanism: membrane translocation mediated by CPP and endocytosis facilitated by nanoparticle formation with ***DS***. This strategy aligns with previous studies demonstrating the efficacy

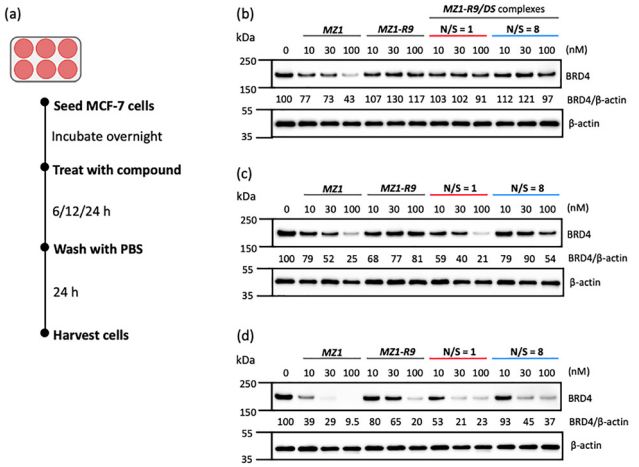

Fig. 4 (a) Experimental workflow for western blot analysis of BRD4 degradation by ***MZ1-R9*** and its ***DS*** complexes (N/S = 1 and N/S = 8). Protein expression levels were quantified using anti-BRD4 and anti-β-actin antibodies. Numbers below the BRD4 bands indicate the BRD4/β-actin ratio, normalized to the vehicle control (set to 100%). MCF-7 cells were treated for (b) 6 h, (c) 12 h, and (d) 24 h.

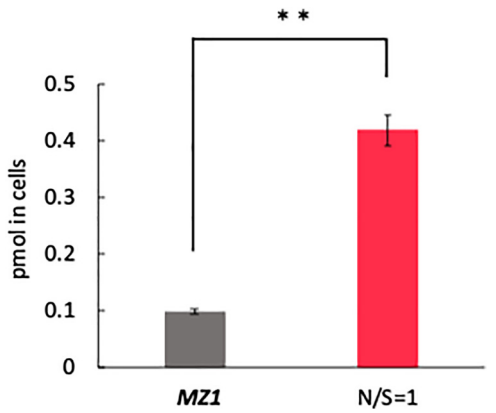

Fig. 5 LC-MS/MS quantification of intracellular ***MZ1*** levels in MCF-7 cells following 12-hour treatment with ***MZ1***, or the ***MZ1-R9/DS*** complex (N/S = 1). Data are presented as mean ± SD (n = 3), $^{**}p < 0.01$.

of CPPs in facilitating PROTAC uptake, including Tat-linked FOXM1 degraders,[27] polyarginine-tagged CREPT degraders,[28] and CPP-fused ERα degraders.[16,17] However, unlike these covalently conjugated systems, our approach leverages noncovalent electrostatic interactions with ***DS***, enabling flexible and modular nanoparticle formation that can be adapted to a variety of PROTAC structures without complex synthetic procedures. Because the conjugation is achieved *via* noncovalent interactions with ***DS***, it allows modular adaptation to various PROTACs without requiring synthetic modification. Compared to other advanced nanodelivery systems, such as POLYPROTACs[29] or LNP-encapsulated bioPROTACs,[30] our ***DS***-based platform offers a simpler and more accessible route for formulation. Unlike LNPs, which require complex formulation and often pose stability issues, or covalent polymer–based systems that demand chemical modification of the PROTAC itself, our noncovalent ***DS***-based approach enables rapid assembly, avoids chemical derivatization, and retains compatibility with diverse PROTAC structures. The resulting nanoparticles possess favorable physicochemical properties, including a hydrodynamic diameter of approximately 90 nm at an N/S ratio of 1 and a moderately positive surface charge, both of which promote efficient cellular uptake *via* multiple endocytic pathways—consistent with previous reports on polyplex-based delivery systems. Despite a marked ∼4-fold increase in intracellular ***MZ1*** concentration achieved with our nanoparticle system, the corresponding enhancement in BRD4 degradation was not proportional. This discrepancy suggests that additional intracellular barriers—such as incomplete endosomal escape, limited nuclear translocation, or suboptimal disulfide cleavage—may hinder effective target engagement and degradation. Several lines of evidence from recent literature support these possible bottlenecks. First, numerous studies have demonstrated that CPP-conjugated macromolecules are often entrapped within endosomes following internalization, resulting in inefficient cytosolic and nuclear delivery.[31,32] Our ***DS***-based nanoparticle system, although effective in facilitating uptake, lacks a dedicated endosomolytic component, which could limit the release of ***MZ1*** into the cytosol and thereby reduce its access to both BRD4 and E3 ligases. In addition, the disulfide linker used for redox-responsive release may cleave too slowly under physiological conditions.[33,34] Our UHPLC data show that approximately 13% of the ***MZ1-R9*** conjugate remained intact after 6 hours in reductive buffer, suggesting that gradual release may limit the availability of active ***MZ1***. Similar release kinetics have been identified as limiting factors in related PROTAC delivery systems.[35] Taken together, these factors may explain why increased cellular ***MZ1*** concentration does not translate linearly to enhanced BRD4 degradation. To address these bottlenecks, future modifications could incorporate endosomolytic motifs, nuclear localization sequences, or dynamic linkers optimized for rapid and efficient intracellular release of the active PROTAC.

In summary, we have developed a modular and redox-responsive nanocomplex platform that significantly improves intracellular delivery and modestly enhances target degradation efficiency. By conjugating the model PROTAC, ***MZ1***, to ***R9*** and assembling the resulting conjugate into nanoparticles with ***DS***, we achieved enhanced intracellular uptake, sustained release, and improved BRD4 degradation *in vitro*. This delivery strategy requires no covalent modification to the carrier polymer, offering versatility and ease of adaptation to other PROTAC structures.

PolyPROTACs and nanocarriers covalently linked to PROTACs achieve controlled release through chemical modification strategies. On the other hand, our modular, electrostatically assembled design, while potentially sensitive to physiological ionic strength and serum conditions, enables the flexible incorporation of diverse functional peptides into a single structure, thereby avoiding complex molecular modifications and enhancing the potential of multifunctional delivery systems. Additionally, the redox-sensitive properties enable the release of cargo under reduced intracellular conditions.

While this platform significantly increases intracellular PROTAC levels, the enhancement in degradation activity was

not strictly proportional, indicating that further optimization—such as endosomal escape enhancers or cleavable linkers tailored for intracellular release—may be necessary. Looking forward, integration of targeting ligands, responsive linkers, or combinatorial payloads may further refine the selectivity and efficacy of this system. Our findings establish a foundational delivery strategy that addresses a critical bottleneck in PROTAC development and opens new avenues for targeting intracellular disease drivers. To address current limitations in intracellular trafficking and degradation, future studies will focus on optimizing cleavable linkers, incorporating endosomal escape enhancers, and evaluating critical factors such as GSH-dependent cleavage efficiency and the potential requirement for nuclear localization in BRD4 degradation.

Conflicts of interest

There are no conflicts to declare.

Data availability

The data supporting this article have been included as part of the SI. See DOI: **https://doi.org/10.1039/d5cb00196j**

Acknowledgements

This study was supported in part by AMED under grant numbers 25mk0121286 and 25ama221127 to Y. D. and JP25am0521016 and JP25mk0121325 to H. Y. This work was also supported by the Japan Society for the Promotion of Science (KAKENHI, grants JP21K05320 and JP23H04926 to Y. D. and JP24K18260 to H. Y.), JST (ACT-X, grant number JPMJAX222L to H. Y.), Takeda Science Foundation to H. Y and Astellas Foundation for Research on Metabolic Disorders to H. Y.

Notes and references

1 K. M. Sakamoto, K. B. Kim, A. Kumagai, F. Mercurio, C. M. Crews and R. J. Deshaies, *Proc. Natl. Acad. Sci. U. S. A.*, 2001, **98**, 8554–8559.
2 M. Malarvannan, S. Unnikrishnan, S. Monohar, V. Ravichandiran and D. Paul, *Bioorg. Chem.*, 2025, **154**, 107984.
3 M. S. Galla, N. Sharma, P. Mishra and N. Shankaraiah, *RSC Med. Chem.*, 2024, **15**, 2585–2600.
4 R. P. Bhole, S. Labhade and S. S. Gurav, *Bioanalysis*, 2025, **17**, 455–470.
5 S. M. Gough, J. J. Flanagan, J. Teh, M. Andreoli, E. Rousseau, M. Pannone, M. Bookbinder, R. Willard, K. Davenport, E. Bortolon, G. Cadelina, D. Gordon, J. Pizzano, J. Macaluso, L. Soto, J. Corradi, K. Digianantonio, I. Drulyte, A. Morgan, C. Quinn, M. Bekes, C. Ferraro, X. Chen, G. Wang, H. Dong, J. Wang, D. R. Langley, J. Houston, R. Gedrich and I. C. Taylor, *Clin. Cancer Res.*, 2024, **30**, 3549–3563.
6 J. S. Scott, I. N. Michaelides and M. Schade, *RSC Med. Chem.*, 2025, **16**, 449–456.
7 A. Pike, B. Williamson, S. Harlfinger, S. Martin and D. F. McGinnity, *Drug Discovery Today*, 2020, **25**, 1793–1800.
8 M. Zengerle, K. H. Chan and A. Ciulli, *ACS Chem. Biol.*, 2015, **10**, 1770–1777.
9 V. G. Klein, C. E. Townsend, A. Testa, M. Zengerle, C. Maniaci, S. J. Hughes, K. H. Chan, A. Ciulli and R. S. Lokey, *ACS Med. Chem. Lett.*, 2020, **11**, 1732–1738.
10 H. Yokoo, M. Naito and Y. Demizu, *Expert Opin. Drug Discovery*, 2023, **18**, 357–361.
11 V. G. Klein, A. G. Bond, C. Craigon, R. S. Lokey and A. Ciulli, *J. Med. Chem.*, 2021, **64**, 18082–18101.
12 M. Oba and Y. Demizu, *Cell-Penetrating Peptides: Design, Development and Applications*, Wiley-VCH, Weinheim, 2022, DOI: **10.1002/9783527835997**.
13 A. Gori, G. Lodigiani, S. G. Colombarolli, G. Bergamaschi and A. Vitali, *ChemMedChem*, 2023, **18**, e202300236.
14 M. Pirhaghi, F. Mamashli, F. Moosavi-Movahedi, P. Arghavani, A. Amiri, B. Davaeil, M. Mohammad-Zaheri, Z. Mousavi-Jarrahi, D. Sharma, U. Langel, D. E. Otzen and A. A. Saboury, *Mol. Pharm.*, 2024, **21**, 2097–2117.
15 B. Zhang, M. Wang, L. Sun, J. Liu, L. Yin, M. Xia, L. Zhang, X. Liu and Y. Cheng, *J. Med. Chem.*, 2024, **67**, 11469–11487.
16 H. Yokoo, N. Ohoka, M. Takyo, T. Ito, K. Tsuchiya, T. Kurohara, K. Fukuhara, T. Inoue, M. Naito and Y. Demizu, *Int. J. Mol. Sci.*, 2021, **22**, 8772.
17 H. Yokoo, N. Ohoka, M. Naito and Y. Demizu, *Bioorg. Med. Chem.*, 2020, **28**, 115595.
18 J. Jin, Y. Wu, J. Chen, Y. Shen, L. Zhang, H. Zhang, L. Chen, H. Yuan, H. Chen, W. Zhang and X. Luan, *Theranostics*, 2020, **10**, 10141–10153.
19 Y. Yu, W. Hu, Y. Xu, H. B. Xu and J. Gao, *J. Control Release*, 2025, **382**, 113719.
20 L. Fang, R. Zhu, M. Li, J. Ma, S. Fan, X. He, Z. Yang, Y. Yan, X. Ma and G. Xiang, *Eur. J. Pharm. Biopharm.*, 2025, **210**, 114699.
21 R. Verma, N. Minocha, V. Mittal and D. Kaushik, *Curr. Drug Ther.*, 2025, **20**, 280–297.
22 Y. Hayashi, J. Yamauchi, I. A. Khalil, K. Kajimoto, H. Akita and H. Harashima, *Int. J. Pharm.*, 2011, **419**, 308–313.
23 S. Futaki and I. Nakase, *Acc. Chem. Res.*, 2017, **50**, 2449–2456.
24 S. Ramasundaram, G. Saravanakumar, S. Sobha and T. H. Oh, *Int. J. Mol. Sci.*, 2022, **24**, 355.
25 S. Guo, X. Zhang, M. Zheng, X. Zhang, C. Min, Z. Wang, S. H. Cheon, M. H. Oak, S. Y. Nah and K. M. Kim, *Biochim. Biophys. Acta*, 2015, **1848**, 2101–2110.
26 M. Oba and M. Tanaka, *Biol. Pharm. Bull.*, 2012, **35**, 1064–1068.
27 K. Wang, X. Dai, A. Yu, C. Feng, K. Liu and L. Huang, *J. Exp. Clin. Cancer Res.*, 2022, **41**, 289.
28 D. Ma, Y. Zou, Y. Chu, Z. Liu, G. Liu, J. Chu, M. Li, J. Wang, S. Y. Sun and Z. Chang, *Theranostics*, 2020, **10**, 3708–3721.

29 J. Gao, B. Hou, Q. Zhu, L. Yang, X. Jiang, Z. Zou, X. Li, T. Xu, M. Zheng, Y. H. Chen, Z. Xu, H. Xu and H. Yu, *Nat. Commun.*, 2022, **13**, 4318.
30 A. Chan, R. M. Haley, M. A. Najar, D. Gonzalez-Martinez, L. J. Bugaj, G. M. Burslem, M. J. Mitchell and A. Tsourkas, *Nat. Commun.*, 2024, **15**, 5808.
31 S. L. Y. Teo, J. J. Rennick, D. Yuen, H. Al-Wassiti, A. P. R. Johnston and C. W. Pouton, *Nat. Commun.*, 2021, **12**, 3721.
32 A. Klipp, M. Burger and J. C. Leroux, *Adv. Drug Delivery Rev.*, 2023, **200**, 115047.
33 A. Nguyen, R. Bottger and S. D. Li, *Biomaterials*, 2021, **275**, 120955.
34 W. Ma, X. Wang, D. Zhang and X. Mu, *Int. J. Nanomed.*, 2024, **19**, 7547–7566.
35 E. W. Syahputra, H. Lee, H. Cho, H. J. Park, K. S. Park and D. Hwang, *Pharmaceutics*, 2025, **17**, 501.